NANO LETTERS

Letter

pubs.acs.org/NanoLett

High-Precision Nanoscale Temperature Sensing Using Single Defects in Diamond

P. Neumann,*[,†] I. Jakobi,[†] F. Dolde,[†] C. Burk,[†] R. Reuter,[†] G. Waldherr,[†] J. Honert,[†] T. Wolf,[†] A. Brunner,[†] J. H. Shim,[‡] D. Suter,[‡] H. Sumiya,[§] J. Isoya,[∥] and J. Wrachtrup[†]

[†]3rd Physikalisches Institut, Research Center Scope and IQST, University of Stuttgart, 70569 Stuttgart, Germany

[‡]Experimentelle Physik III, Universität Dortmund, 44221 Dortmund, Germany

[§]Sumitomo Electric Industries, Ltd., Itami, Hyogo, 664-0016 Japan

[∥]Research Center for Knowledge Communities, University of Tsukuba, Tsukuba, Ibaraki, 305-8550 Japan

S *Supporting Information*

ABSTRACT: Measuring local temperature with a spatial resolution on the order of a few nanometers has a wide range of applications in the semiconductor industry and in material and life sciences. For example, probing temperature on the nanoscale with high precision can potentially be used to detect small, local temperature changes like those caused by chemical reactions or biochemical processes. However, precise nanoscale temperature measurements have not been realized so far owing to the lack of adequate probes. Here we experimentally demonstrate a novel nanoscale temperature sensing technique based on optically detected electron spin resonance in single atomic defects in diamonds. These diamond sensor sizes range from a micrometer down to a few tens of nanometers. We achieve a temperature noise floor of 5 mK/Hz$^{1/2}$ for single defects in bulk sensors. Using doped nanodiamonds as sensors the temperature noise floor is 130 mK/Hz$^{1/2}$ and accuracies down to 1 mK for nanocrystal sizes and therefore length scales of a few tens of nanometers. This combination of precision and position resolution, combined with the outstanding sensor photostability, should allow the measurement of the heat produced by chemical interactions involving a few or single molecules even in heterogeneous environments like cells.

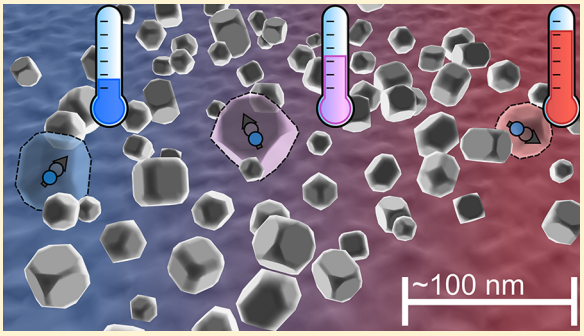

KEYWORDS: *Nanoscale, temperature measurement, diamond, spin defect, NV center*

Several kinds of nanoscale temperature sensing techniques have been developed in the recent past.[1] These are scanning thermal microscopes (SThM),[2] dispersed or scanned fluorescent nanoprobes,[3−5] probe-free methods like micro-Raman spectroscopy,[6] or near-field optical temperature measurements.[7] SThMs have temperature-sensitive elements at a scanning tip (e.g., thermocouple) and are invasive. Dispersed fluorescent nanoprobes have the advantage of operation without direct contact and can have much higher precision than the Raman or near-field probes. In the fluorescent nanoprobes temperature-dependent properties (e.g., distortion of the fluorescence spectrum) are exploited to achieve high sensitivity.

In this study we utilize a fluorescent temperature probe consisting of a single quantum system in a solid state matrix, namely, the negatively charged nitrogen-vacancy (NV) center in diamond, which allows probe sizes down to ∼5 nm.[8] This system has been studied for other applications like quantum information processing using high fidelity control of its ground state electronic and nuclear spins.[9−14] It has also been used for several nanometer-scale metrology purposes[15−18] like measuring small magnetic and electric fields. Here we show that the NV also allows tracking of temperature with high precision. These NV temperature nanoprobes can be either dispersed in the specimen to be investigated or used in a scanning probe geometry (see Figure 1a).

The NV center is a molecular impurity in the diamond crystal comprised of a substitutional nitrogen impurity adjacent to a carbon vacancy. Optical excitation in a wavelength range from 460 to 580 nm yields intense fluorescence emission.[19] Excitation also leads to a high degree of ground state electron spin polarization, namely, the m_S = 0 sublevel ($|0\rangle$) of the ground state electron spin triplet.[20] Furthermore the fluorescence decreases upon spin flips into the m_S = ±1 sublevels ($|\pm\rangle$) allowing optically detected magnetic resonance (ODMR) experiments of single NV spins at room temperature.[21] The NV ground state spins possess long coherence times (∼1 ms),[11,22] and this enables the high fidelity needed for coherent control and metrology applications. In addition there is a detectable temperature dependence of the electron spin

Received: April 4, 2013
Revised: May 22, 2013
Published: May 30, 2013

dx.doi.org/10.1021/nl401216y | *Nano Lett.* 2013, 13, 2738−2742

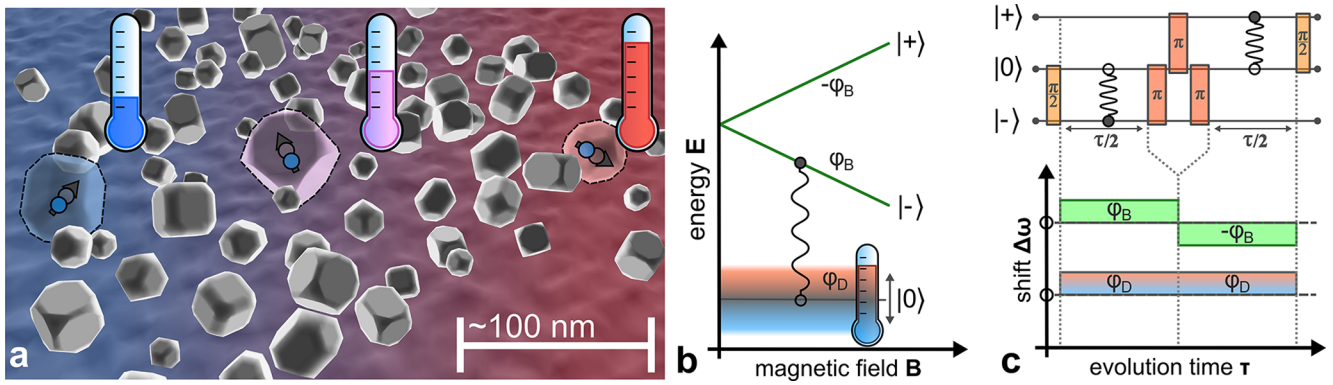

Figure 1. NV thermometer operation scheme. (a) Nanodiamonds containing single NV centers can serve as distributed probe temperature sensors. (b) Electron spin energy levels are mainly influenced by applied axial magnetic fields B_z and the temperature T. B_z splits the levels $|\pm\rangle$ and the temperature shifts level $|0\rangle$ with respect to $|\pm\rangle$. During free evolution the spin states acquire phases φ_D, φ_B, and $-\varphi_B$. The initial superposition state $|0\rangle+|-\rangle$ of our excitation sequence is depicted. (c) D-Ramsey sequence to cancel the magnetic signal. The upper part shows mw pulses for spin control and the resulting spin coherences. The lower part shows phase cancellation and accumulation for magnetic (B) and temperature (T) contributions.

resonance frequency from temperatures of around 120 K[23,24] up to 700 K.[25]

Single NV centers in either a bulk diamond sample or nanodiamonds are probed by optical excitation with 532 nm laser light and fluorescence collection with a confocal microscope. Microwave (mw) radiation for spin manipulation is applied by an appropriate wire close to the NV position. The ODMR spectrum of the NV center spin usually comprises two resonance lines corresponding to spin transitions between levels $|0\rangle \leftrightarrow |-\rangle$ and $|0\rangle \leftrightarrow |+\rangle$[21] (see Supporting Information). These spin levels depend on external parameters like magnetic (B) and electric fields, temperature T, and strain (see Figure 1b). By analyzing the spin Hamiltonian

$$H = D(T)S_z^2 + \gamma_{NV}(B_zS_z + B_xS_x + B_yS_y) + H_{hf} + H_{nuc} \quad (1)$$

one can distinguish between the individual contributions. In Figure 1b the first two largest terms of eq 1 are illustrated. These are the crystal field which splits spin state $|0\rangle$ from states $|\pm\rangle$ and the Zeeman term due to axial magnetic field B_z which splits states $|\pm\rangle$. The latter terms commute. The crystal field parameter D depends on temperature T, axial electric field, and strain. Under ambient conditions the temperature dependence is $c_T = dD/dT = -74.2$ kHz/K.[23] By utilizing a dedicated coherent control technique like in Figure 1c we reduce contributions from axial magnetic fields, electric fields, and strain which are therefore neglected in eq 1. The next smaller terms in the Hamiltonian are the transverse magnetic fields (B_x, B_y) which do not commute with the previous ones. Transverse fields split levels $|\pm\rangle$ and additionally shift them with respect to $|0\rangle$. Therefore they can be confused with temperature changes. Sufficiently strong axial magnetic fields suppress the effect of small transverse magnetic fields. Eventually, each electron spin level is split by a hyperfine interaction

$$H_{hf} = \sum_{j=\text{spins}} \sum_{i=x,y,z} S_z A_{zi}^j I_i^j \quad (2)$$

to the nitrogen nuclear spin of the NV ($^{14}N \rightarrow I = 1$, $^{15}N \rightarrow I = 1/2$)[26] and is inhomogeneously broadened by the ^{13}C nuclear spin bath.[22,27] Other minor broadening effects are impurity electron spins in the diamond lattice or fluctuating electric or magnetic fields. In diamonds with natural abundance of ^{13}C the inhomogeneous ODMR line width is $1/T_2^* \sim 1$ MHz. This broad line width has severely limited temperature sensitivity in previous measurements where line shifts were used to measure temperature.[23−25,28]

Following the above analysis of the spin Hamiltonian we adapt our experiments accordingly. The noncommuting terms in eq 1, that is, mainly the effect of transverse magnetic fields, are suppressed by a magnetic field of ≈50 mT aligned along the NV axis (i.e., $B = B_z$), as already mentioned above. To suppress parasitic effects from commuting terms, for example, axial electric fields due to lattice defects, we use type IIa synthetic HPHT diamonds with low nitrogen content (<14 ppb, see Supporting Information). Additionally, we have developed a special decoupling sequence (see Figure 1c). As mentioned above this cancels axial magnetic sensitivity and therefore eliminates resonance line broadening due to axial magnetic interactions with, for example, spin impurities. At the same time sensitivity to changes in D (i.e., temperature) is maintained.

As illustrated in Figure 1c we first create a superposition state $|0\rangle + |-\rangle$ which acquires a phase $\varphi_B - \varphi_D$ during time $\tau/2$, $(e^{-i\varphi_D}|0\rangle + e^{-i\varphi_B}|-\rangle)$. Next, this state is converted to $e^{-i\varphi_D}|0\rangle - e^{-i\varphi_B}|+\rangle$ and acquires an additional phase $-\varphi_B - \varphi_D$ during time $\tau/2$, $(e^{-i2\varphi_D}|0\rangle - |+\rangle)$. The total phase $-2\varphi_D = \Delta D \cdot \tau$ is proportional to shifts of D only. ΔD is defined as an average change of D with respect to an initial value which is assumed to be in resonance with the applied mw frequencies. All intermediate phases φ_B caused by quasistatic fluctuations of magnetic field are canceled. Eventually, the NV fluorescence is modulated with $\cos(2\pi\Delta D\tau)$, that is, a D-Ramsey oscillation with frequency ΔD for increasing phase accumulation time τ (see Figure 2b bottom). The decay time T_D of this oscillation is up to ∼1 ms corresponding to a homogeneous broadening of $1/T_D \sim 1$ kHz. Therefore we increase the phase accumulation time τ by orders of magnitude from T_2^* to T_D which in turn improves the frequency (temperature) uncertainty. Similar decoupling techniques for low magnetic fields have been theoretically proposed recently.[29]

The nuclear spin bath (see eq 2) does not only lead to quasistatic fluctuating magnetic fields but additionally leads to entanglement between the bath spins and the electron spin.[27,30] The latter effect also appears during echo sequences and effectively leads to faster decoherence. The main requirement for this entanglement is that A_{zx} and A_{zy} terms of the hyperfine

dx.doi.org/10.1021/nl401216y | Nano Lett. 2013, 13, 2738−2742

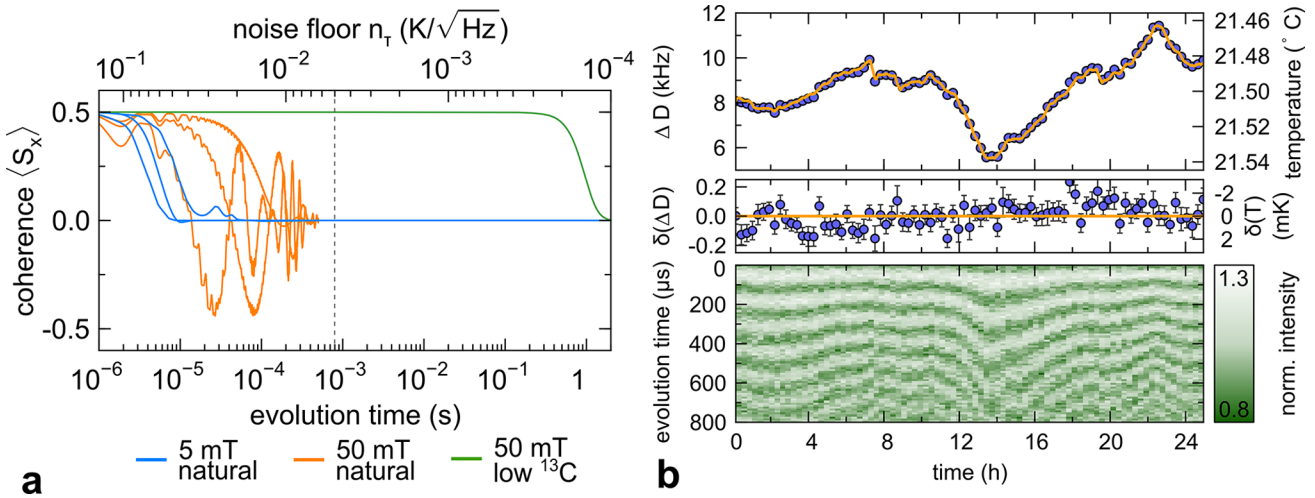

Figure 2. NV bulk diamond temperature sensor. (a) Simulation of *D*-Ramsey coherence decays for different ^{13}C concentrations and axial magnetic fields: c = 0.01 and B_z = 5 mT (blue), c = 0.01 and B_z = 50 mT (orange), and $c = 10^{-5}$ and B_z = 50 mT (green). The multiple curves for each case (color) originate from different ^{13}C distributions in the lattice which are randomly chosen for each simulation. Only decoherence due to the nuclear spin bath has been considered. The experimentally obtained coherence time and the corresponding temperature noise floor are marked as vertical dashed lines. This correlation is setup-dependent. (b) Bottom part shows consecutive *D*-Ramsey oscillations (vertical slices) of a single NV center. The oscillation frequency is proportional to the temperature change. Vertical and horizontal axes are free evolution time τ of the *D*-Ramsey and total measurement time t, respectively. The fluorescence response is color coded. Upper part shows the crystal field parameter D = 2870.685 MHz + ΔD and temperature T (circles) deduced from the *D*-Ramsey oscillation frequency (bottom). In addition the temperature T of the diamond measured by a thermistor is plotted (orange curve). We obtain a temperature dependence $c_T = -78.6 \pm 0.5$ kHz/K. The middle part shows difference between NV temperature results and thermistor measured temperature, that is, the difference between blue circles and orange line in the top part ($\delta(\Delta D)$,δT).

interaction are comparable with the nuclear Zeeman energy (see H_{hf} and H_{nuc} in eq 2 and the Supporting Information). We face this obstacle by reducing the ^{13}C concentration for the HPHT bulk diamond samples and by increasing the magnetic field which reduces the number of bath spins for which the above-mentioned requirement is fulfilled. The effect of these two countermeasures can be estimated by numerically simulating the *D*-Ramsey decay due to the spin bath using the cluster expansion method[27] (see Supporting Information). Figure 2a shows the expected *D*-Ramsey decay for a few magnetic field and ^{13}C concentration settings. The reduction of the ^{13}C concentration and the increase of the magnetic field obviously lead to an increase of coherence time by more than 2 orders of magnitude and are therefore essential.

Our experiments are divided into two parts. In the first part we test our novel *D*-Ramsey sequence for single NV centers ≈1 μm below the bulk diamond surface, to explore the best temperature sensitivity achievable. In the second part we use NV centers in nanodiamonds as nanoscale sensors to measure temperature changes as a function of distance to a microstructure used as a local heat source.

In the first part (see Figure 2b bottom) we consecutively measured full *D*-Ramsey oscillations for one day to track temperature and possible other effects on *D*. Figure 2b top shows the crystal field parameter *D* calculated from the *D*-Ramsey oscillations' frequencies. In addition the temperature was measured by a thermistor close to the diamond (see Supporting Information). For a value $c = -78.6 \pm 0.5$ kHz/K both results coincide (see Figure 2b, middle). The average decay time of the *D*-Ramsey oscillations is $T_D = 829 \pm 24$ μs for measurement intervals of 17 min per point. This corresponds to variations of the crystal field parameter *D* of ±0.2 kHz during one measurement interval. Hence, temperature variations during one interval are at least within ±2.5 mK. Frequency uncertainties of fits to the *D*-Ramsey oscillations yield uncertainties of 1 mK (see error bars) for the average temperature during one interval. For the difference between NV-based and thermistor-based temperature data ($\delta(\Delta D)$ and δT in Figure 2b, middle) we obtain a standard deviation of 1 mK. Our sensor therefore exhibits sufficient long-term stability.

Furthermore we have investigated the influence of laser and microwave heating during this measurement sequence by artificially increasing the average heating power of the laser and microwave. We found that the microwave radiation has a negligible effect of much less than 1 mK while the laser heats the sample by less than 3 mK on average.

As mentioned above, Figure 2b bottom shows full *D*-Ramsey oscillations. However the highest temperature sensitivity is only achieved for longest phase accumulation times τ. Taking into account only measurements with τ = 800 μs, we have achieved a temperature noise floor of $n_T \approx 5$ mK/Hz$^{1/2}$ for a maximum measurement rate $r \approx 1$ Hz. For a given r the uncertainty of each measurement point is $\sigma_T = n_T r^{1/2}$. The noise floor and the maximum measurement rate depend on τ approximately as $1/\tau^{1/2}$ and $1/\tau$, respectively.

In a second set of experiments NV centers in nanodiamonds were used. We prepared a glass cover slide with a microstructured loop-gap resonator with a resonance frequency of ≈1.8 GHz and a line width of ≈200 MHz (see Figure 3b inset) which can be excited from a distance via radiofrequency (rf) radiation. Afterward nanodiamonds with a nominal size of 50 nm containing naturally occurring NV centers (see Supporting Information) were put in polyvinyl alcohol (PVA) and then spin-coated on top of this slide (see Figure 3a). Single NV centers were addressed by a confocal microscope, and their temperature response was investigated.

Checks of the T_2 time and the *D*-Ramsey lifetime of the nanodiamonds yielded values in the range of 1−5 μs. Next we

dx.doi.org/10.1021/nl401216y | Nano Lett. 2013, 13, 2738−2742

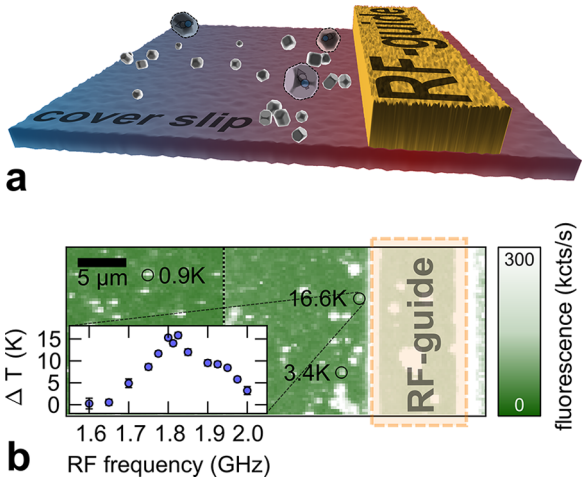

Figure 3. Nanodiamonds as temperature probes. (a) Schematics of the experiment. Nanodiamonds are scattered across a glass cover slide. A microstructured loop-gap resonator (partially shown as rf-guide) can be heated by rf radiation. In the region of the current antinode the resonator dissipates energy due to ohmic loss, heating the underlying glass slide. Confocal imaging was performed from below the glass slide. (b) Lateral confocal microscopy scan showing individual NV centers and part of the loop-gap resonator. The local temperature has been measured for three different distances from the resonator (black circles). (inset) Temperature shift of a single nanodiamond close to the wire depends on the rf frequency used to excite the resonator. This frequency dependence agrees with the resonance response of the resonator.

heated the sample uniformly to check for the homogeneity of the temperature scaling c_T among the nanodiamonds. For several tens of NV nanodiamonds we found slight variations which we equate to our measurement accuracy. Next we applied our NV nanoscale thermometers to measure heating by the microstructure antenna. To this end we measured temperature changes close to the microstructure wire using a single NV center in a nanodiamond (see Figure 3b). The temperature change versus the excitation frequency of the microstructure clearly reveals its resonance (see Figure 3b inset). When increasing the distance between the nanodiamond and the micro resonator by a few micrometers the temperature changes decrease (see Figure 3b).

The measured temperature does not exactly coincide with our expectation of a heated gold wire in thermal contact with a glass substrate. The main reason for this discrepancy is believed to be the unknown thermal coupling of the nanodiamonds to the glass substrate which is modified by an unknown and varying thickness of PVA.

The temperature noise floor reached in the nanodiamond experiment is $n_T \approx 130$ mK/Hz$^{1/2}$, that is, larger than for the bulk sample because of the shorter T_D value. This however allows for faster maximum measurement rates of $r \approx 100$ Hz.

Utilizing our novel decoupling scheme with NV diamond a significant increase in temperature sensitivity is seen. In bulk, we find the long-term accuracy of the sensor is 1 mK. In addition we demonstrate enhanced sensitivity for NV nanodiamonds achieving similar sensitivities to those recently reported for bulk samples.[25] Such nanodiamonds can be used as distributed temperature probes to reveal spatially resolved temperature profiles with spatial resolution only limited by their size.

Results closely related to this work have been reported very recently.[31,32] Toyli et al. concentrated on higher order decoupling schemes,[31] and Kucsko et al. investigated biological applications.[32]

Temperature sensitivity can be further improved by a higher photon collection efficiency, for example, by solid immersion lenses[33] or diamond pillar structures.[34] In addition T_D can be improved by analogues of higher order dynamical decoupling sequences like CPMG or UDD[31,35] allowing for micro Kelvin temperature sensitivity.

Our results pave the way for implementing NV diamond temperature sensors for material and life sciences. One might imagine the integration of NV centers into diamond AFM cantilever tips.[18] As distributed probes the selective attachment of nanodiamonds to specific parts of living cells or material and device parts seems feasible.[36] While the temperature dependence of D vanishes for temperatures below about 120 K, other temperature-dependent properties of the NV center, like the zero-phonon line position of the fluorescence spectrum, become accessible.

For temperature measurements with higher time resolution pump probe measurements can be performed. To this end the timing of heat generation and the temperature measurement sequence need to be properly synchronized. As diamond has one of the highest heat conductivities fast thermal response is expected.

■ ASSOCIATED CONTENT

Supporting Information

A more thorough description of the spin Hamiltonian, HPHT and nanodiamond samples, experimental setup, and simulations of nuclear spin bath influences. This material is available free of charge via the Internet at http://pubs.acs.org.

■ AUTHOR INFORMATION

Corresponding Author

*E-mail: p.neumann@physik.uni-stuttgart.de.

Notes

The authors declare no competing financial interest.

■ ACKNOWLEDGMENTS

We thank Fedor Jelezko, Ilja Gerhardt, Philip Hemmer, and Julia Michl for discussion. We would like to acknowledge financial support by DFG and JST (SFB-TR 21, FOR 1482), EU (DIAMANT), and Baden-Württemberg Stiftung gGmbH ("Methoden für die Lebenswissenschaften"). A.B. acknowledges support by the Hans L. Merkle-Stiftung.

■ REFERENCES

(1) Yue, Y.; Wang, X. *Nano Rev.* **2012**, 3.
(2) Majumdar, A. *Annu. Rev. Mater. Sci.* **1999**, *29*, 505−585.
(3) Vetrone, F.; Naccache, R.; Zamarrón, A.; Juarranz de la Fuente, A.; Sanz-Rodríguez, F.; Martinez Maestro, L.; Martín Rodriguez, E.; Jaque, D.; García Solé, J.; Capobianco, J. A. *ACS Nano* **2010**, *4*, 3254−3258.
(4) Aigouy, L.; Tessier, G.; Mortier, M.; Charlot, B. *Appl. Phys. Lett.* **2005**, *87*, 184105−184105−3.
(5) Okabe, K.; Inada, N.; Gota, C.; Harada, Y.; Funatsu, T.; Uchiyama, S. *Nat. Commun.* **2012**, *3*, 705.
(6) Beechem, T.; Graham, S.; Kearney, S. P.; Phinney, L. M.; Serrano, J. R. *Rev. Sci. Instrum.* **2007**, *78*, 061301−061301−9.
(7) Christofferson, J.; Maize, K.; Ezzahri, Y.; Shabani, J.; Wang, X.; Shakouri, A. *J. Electron. Pack.* **2008**, *130*, 041101.
(8) Tisler, J.; et al. *ACS Nano* **2009**, *3*, 1959−1965.

(9) Jelezko, F.; Gaebel, T.; Popa, I.; Domhan, M.; Gruber, A.; Wrachtrup, J. *Phys. Rev. Lett.* **2004**, *93*, 130501.
(10) Dutt, M. V. G.; Childress, L.; Jiang, L.; Togan, E.; Maze, J.; Jelezko, F.; Zibrov, A. S.; Hemmer, P. R.; Lukin, M. D. *Science* **2007**, *316*, 1312−1316.
(11) Neumann, P.; Mizuochi, N.; Rempp, F.; Hemmer, P.; Watanabe, H.; Yamasaki, S.; Jacques, V.; Gaebel, T.; Jelezko, F.; Wrachtrup, J. *Science* **2008**, *320*, 1326−1329.
(12) Shi, F.; Rong, X.; Xu, N.; Wang, Y.; Wu, J.; Chong, B.; Peng, X.; Kniepert, J.; Schoenfeld, R.-S.; Harneit, W.; Feng, M.; Du, J. *Phys. Rev. Lett.* **2010**, *105*, 040504.
(13) Neumann, P.; Beck, J.; Steiner, M.; Rempp, F.; Fedder, H.; Hemmer, P. R.; Wrachtrup, J.; Jelezko, F. *Science* **2010**, *329*, 542−544.
(14) Dolde, F.; Jakobi, I.; Naydenov, B.; Zhao, N.; Pezzagna, S.; Trautmann, C.; Meijer, J.; Neumann, P.; Jelezko, F.; Wrachtrup, J. *Nat. Phys.* **2013**, *9*, 139−143.
(15) Maze, J. R.; Stanwix, P. L.; Hodges, J. S.; Hong, S.; Taylor, J. M.; Cappellaro, P.; Jiang, L.; Dutt, M. V. G.; Togan, E.; Zibrov, A. S.; Yacoby, A.; Walsworth, R. L.; Lukin, M. D. *Nature* **2008**, *455*, 644−647.
(16) Balasubramanian, G.; Chan, I. Y.; Kolesov, R.; Al-Hmoud, M.; Tisler, J.; Shin, C.; Kim, C.; Wojcik, A.; Hemmer, P. R.; Krueger, A.; Hanke, T.; Leitenstorfer, A.; Bratschitsch, R.; Jelezko, F.; Wrachtrup, J. *Nature* **2008**, *455*, 648−651.
(17) Dolde, F.; Fedder, H.; Doherty, M. W.; Nobauer, T.; Rempp, F.; Balasubramanian, G.; Wolf, T.; Reinhard, F.; Hollenberg, L. C. L.; Jelezko, F.; Wrachtrup, J. *Nat. Phys.* **2011**, *7*, 459−463.
(18) Maletinsky, P.; Hong, S.; Grinolds, M. S.; Hausmann, B.; Lukin, M. D.; Walsworth, R. L.; Loncar, M.; Yacoby, A. *Nat. Nanotechnol.* **2012**, *7*, 320−324.
(19) Aslam, N.; Waldherr, G.; Neumann, P.; Jelezko, F.; Wrachtrup, J. *New J. Phys.* **2013**, *15*, 013064.
(20) Waldherr, G.; Beck, J.; Steiner, M.; Neumann, P.; Gali, A.; Frauenheim, T.; Jelezko, F.; Wrachtrup, J. *Phys. Rev. Lett.* **2011**, *106*, 157601.
(21) Gruber, A.; Drabenstedt, A.; Tietz, C.; Fleury, L.; Wrachtrup, J.; vonBorczyskowski, C. *Science* **1997**, *276*, 2012−2014.
(22) Mizuochi, N.; Neumann, P.; Rempp, F.; Beck, J.; Jacques, V.; Siyushev, P.; Nakamura, K.; Twitchen, D.; Watanabe, H.; Yamasaki, S.; Jelezko, F.; Wrachtrup, J. *Phys. Rev. B* **2009**, *80*, 041201.
(23) Acosta, V. M.; Bauch, E.; Ledbetter, M. P.; Waxman, A.; Bouchard, L.-S.; Budker, D. *Phys. Rev. Lett.* **2010**, *104*, 070801.
(24) Chen, X.-D.; Dong, C.-H.; Sun, F.-W.; Zou, C.-L.; Cui, J.-M.; Han, Z.-F.; Guo, G.-C. *Appl. Phys. Lett.* **2011**, *99*, 161903−161903−3.
(25) Toyli, D. M.; Christle, D. J.; Alkauskas, A.; Buckley, B. B.; Van de Walle, C. G.; Awschalom, D. D. *Phys. Rev. X* **2012**, *2*, 031001.
(26) Rabeau, J. R.; Reichart, P.; Tamanyan, G.; Jamieson, D. N.; Prawer, S.; Jelezko, F.; Gaebel, T.; Popa, I.; Domhan, M.; Wrachtrup, J. *Appl. Phys. Lett.* **2006**, *88*, 023113.
(27) Maze, J.; Taylor, J.; Lukin, M. *Phys. Rev. B* **2008**, 78.
(28) Bouchard, L.-S.; Acosta, V. M.; Bauch, E.; Budker, D. *New J. Phys.* **2011**, *13*, 025017.
(29) Hodges, J. S.; Yao, N. Y.; Maclaurin, D.; Rastogi, C.; Lukin, M. D.; Englund, D. *Phys. Rev. A* **2013**, *87*, 032118.
(30) Childress, L.; Gurudev Dutt, M. V.; Taylor, J. M.; Zibrov, A. S.; Jelezko, F.; Wrachtrup, J.; Hemmer, P. R.; Lukin, M. D. *Science* **2006**, *314*, 281−285.
(31) Toyli, D. M.; de Las Casas, C. F.; Christle, D. J.; Dobrovitski, V. V.; Awschalom, D. D. *Proc. Natl. Acad. Sci. U.S.A.* **2013**, *110*, 8417−8421.
(32) Kucsko, G.; Maurer, P. C.; Yao, N. Y.; Kubo, M.; Noh, H. J.; Lo, P. K.; Park, H.; Lukin, M. D. *arXiv:1304.1068* **2013**.
(33) Marseglia, L.; Hadden, J. P.; Stanley-Clarke, A. C.; Harrison, J. P.; Patton, B.; Ho, Y.-L. D.; Naydenov, B.; Jelezko, F.; Meijer, J.; Dolan, P. R.; Smith, J. M.; Rarity, J. G.; O'Brien, J. L. *Appl. Phys. Lett.* **2011**, *98*, 133107−133107-3.
(34) Babinec, T. M.; Hausmann, B. J. M.; Khan, M.; Zhang, Y.; Maze, J. R.; Hemmer, P. R.; Lončar, M. *Nat. Nanotechnol.* **2010**, *5*, 195−199.
(35) Lange, G. d.; Wang, Z. H.; Ristè, D.; Dobrovitski, V. V.; Hanson, R. *Science* **2010**, *330*, 60−63.
(36) Krueger, A.; Lang, D. *Adv. Funct. Mater.* **2012**, *22*, 890−906.